Hindawi
Advances in Civil Engineering
Volume 2022, Article ID 7796204, 18 pages
https://doi.org/10.1155/2022/7796204

Research Article

Reduction of Vibrations in Long-Span Continuous Girder Bridges with Pounding Tuned Mass Dampers

Juncheng Yao,[1,2] Hekuan Zhou,[3] Jiahua Zhu,[4] Liang Huang ,[1] Jianguo Xu,[1] and Weiguo Li[3]

[1]*School of Water Conservancy and Civil Engineering, Zhengzhou University, Zhengzhou 450001, China*
[2]*CCCC Second Highway Consultants Co., Ltd., Wuhan 430056, China*
[3]*Highway Engineering Bureau Group Co., Ltd. of Henan Province, Zhengzhou 450052, China*
[4]*CCCC Infrastructure Maintenance Group Co., Ltd., Guangzhou Branch, Guangzhou 510220, China*

Correspondence should be addressed to Liang Huang; zzuhuangliang@163.com

Received 12 July 2022; Accepted 3 September 2022; Published 3 October 2022

Academic Editor: Chao Zou

Earthquakes often cause bridges to vibrate to different degrees; moreover, in the case of poor road conditions, the vibration amplitude of bridges caused by vehicles often exceeds a reasonable range, thus causing different degrees of damage to bridges. Therefore, this article studies the vibration reduction effect of the pounding tuned mass dampers (PTMD) on long-span continuous bridges under earthquake and vehicle loads. The PTMD used in this study can reduce the vibration in both lateral and vertical directions. The PTMD provides a stronger vibration dampening effect compared to the TMD since it increases collision to use energy. The LS-DYNA software is used for numerical modeling to optimize the parameters of the PTMD and to determine the size and installation position of the PTMD. Then, the bridge is subjected to two recorded ground motions, and the bridge response with and without the PTMD is compared and analyzed, which shows how PTMD might lessen bridge vibration in its transverse direction. To assess how efficiently the PTMD dampens vibrations induced by vehicle loads on bridges, a vehicle/bridge/PTMD system is simulated using a refined vehicle model. The findings demonstrate that the PTMD may significantly lessen the bridge's lateral and vertical vibration while enhancing driving comfort. Thus, this research study is of great significance for vertical and lateral vibration control of long-span continuous girder bridges.

1. Introduction

The bridge structure is an important part of the uninterrupted operation lifeline. At present, there are many existing bridges that mainly consider gravity load and vehicle load in the design, so they are not enough to withstand earthquakes. In previous reports, earthquakes often caused different degrees of damage to bridge structures, so bridge seismic research has been continuously developed [1–4]. As a result, lowering the bridge's seismic response is critical. In the case of poor road conditions, the amplitude of bridge vibration caused by vehicle driving often exceeds a reasonable range. Vehicle weight, speed, and the state of the road's surface all have an impact on how much the bridge vibrates [5–8]. This study's findings indicate that when the road is uneven and the car is heavy, the vibration created by the vehicle on the bridge will frequently be more intense than is appropriate. Therefore, it is necessary to use dampers to control bridge vibration.

Many academics have studied the vibration of structures in-depth [9, 10]. Studying the impact of subway trains on tunnel vibration was performed by Ma et al. [11]. From a theoretical perspective, Xu and Ma investigated the dynamic response of a multilayer half-space under spatial periodic harmonic stresses [12]. A novel impedance model was suggested by Zou et al. to investigate how subway vibration affects nearby structures [13]. Wu et al. presented the "Kriging model + swarm intelligence updating technique" for the finite element model of complex bridges and applied it to the finite element model of complex bridges [14]. Seismic isolation technology is an effective damping measure. Numerous computer calculations and experimental tests have verified the damping effect of seismic isolation technology [9, 10]. Seismic isolation technology usually uses

flexible supports to isolate the upper structure from its foundation, when seismic excitations propagate upward from the foundation, the energy is greatly weakened. Another common control method for reducing bridge vibration is TMD [15]. Many scholars have conducted various optimization studies on TMD according to the actual situation. TMD is widely used in bridge structure vibration reduction [16].

TMD is a passive control device, usually installed in the most responsive position of the structure. If the TMD is constructed properly, it may efficiently absorb energy and lessen the displacement of the bridge when the fundamental frequencies of the TMD and the bridge coincide [17]. Rana and Soong studied the characteristics of TMD parameters and proposed the application of TMD in a multidegree of freedom structures [18]. However, the energy dissipation capability of TMD has certain limitations, and the vibration frequency range of TMD is relatively small. Although TMD was applied to vibration reduction of various engineering structures decades ago, various optimization designs of TMD are still very active [19–31]. In order to further reduce structural vibration, many improved TMDs have been proposed, such as unconventional TMD, granular TMD, and eddy current TMD [32–35].

Recently, Yin et al. used pounding tuned mass dampers (PTMD) to suppress bridge vibration caused by vehicle motion [36]. PTMD is mainly composed of two parts: moving mass and delimiter. The L-shaped steel beam is connected with the mass block and passes through the inner surface of the delimiter. Furthermore, a layer of viscoelastic material is attached to the inner surface of the delimiter. The L-shaped steel beam collides with the viscoelastic material when the structure vibrates, dissipating structural kinetic energy.

Therefore, compared with conventional TMD, PTMD increases energy consumption through collision and therefore has a better vibration control effect. In addition, PTMD can also improve the robustness of the system [37–40]. Because PTMD has a good effect on reducing vibration and is easy to install and maintain, it is often used for vibration reduction in various engineering structures [35–38, 40–44]. Many scholars have applied PTMD in the field of bridge vibration reduction.

Wang et al. studied the damping effects of multiple PTMDs on bridge structures, mainly considering the combined effects of vehicle loads and wind loads [39]. Li et al. proposed single-sided PTMD (SS-PTMD) and further optimized various design parameters. Experiments and computer simulations show that the SS-PTMD can greatly minimize the bridge deck's vortex-induced vibration [40]. Zhang et al. proposed an asymmetric PTMD. The response of cable-stayed bridges under various seismic excitations has been comparatively studied. APTMD has a perfect vibration damping effect [45]. However, there are not many studies on PTMD in suppressing the vibration of continuous beam bridges.

According to [36, 41, 42, 44], this study uses PTMD technology to lessen the lateral and vertical vibration of a long-span continuous girder bridge. This research focuses on the use of PTMD to reduce vibration on bridges subjected to earthquakes and moving vehicle loads. First, the main design parameters of PTMD are optimized. Secondly, two recorded ground motions from the El-Centro and Taft earthquakes are applied laterally to the bridge system with or without PTMD. The impact of the PTMD vibration reduction is then confirmed by comparing and analyzing the dynamic response data. Finally, based on the refined vehicle model, a refined numerical simulation of the bridge-vehicle-PTMD system is carried out. Subsequently, it is assessed how PTMD will impact driving comfort and how much of the system's vertical vibration will be reduced. The research in this study is of great significance for vertical and lateral vibration control of long-span continuous girder bridges. In addition, a refined vehicle model is used in this study, which further improves the accuracy of vehicle-induced bridge vibration studies.

2. Modeling and Basic Theory

2.1. Pounding Tuned Mass Dampers. Figure 1 depicts the composition of the PTMD, which also includes a moving mass, an L-shaped steel beam, and a viscoelastic delimiter. A layer of viscoelastic material is attached to the inner surface of the delimiter. The L-shaped steel beam and mass block are consolidated. The L-shaped steel beam will flex somewhat and will crash onto the inner surface of the delimiter when the structure shakes, thereby dissipating energy and reducing structural vibration [42, 44]. There is an opening inside the delimiter, and a viscoelastic material is attached to the opening of the delimiter. The delimiter is fixed to the main structure. PTMD can reduce the dynamic response in both the vertical direction and the radial direction of the delimiter because the L-shaped rod can only bend in these two directions.

2.2. The Nonlinear Pounding Force Model. When the structure vibrates, the PTMD will run into the limitation. So, it is important to construct a matching numerical model of the collision force in the cause of examining the interaction between the PTMD and the bridge structure. The nonlinear model used in this work combines the Hert contact element and the damper, which has been proved to be one of the most suitable models in previous studies [42].

$$F = \begin{cases} \beta\delta^{3/2} + c\dot{\delta}, \dot{\delta} > 0, \\ \beta\delta^{3/2}, \dot{\delta} < 0, \end{cases} \tag{1}$$

$$\delta = \begin{cases} x_1 - x_2 - g_p, x_1 - x_2 > g_p, \\ \left| x_1 - x_2 - g_p \right|, x_1 - x_2 < -g_p, \\ 0, otherwise, \end{cases} \tag{2}$$

$$\dot{\delta} = \dot{x}_1 - \dot{x}_2,$$
$$c = 2\xi\sqrt{\beta\delta^{1/2}\frac{m_1 m_2}{m_1 + m_2}}. \tag{3}$$

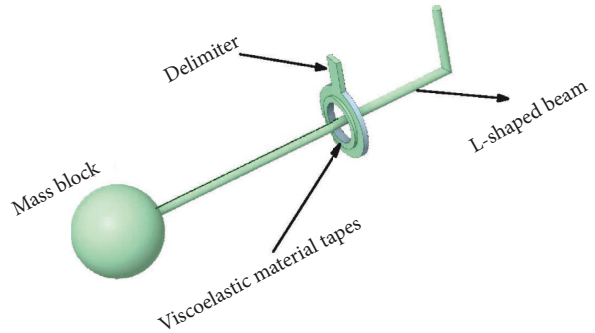

Figure 1: Components of a PTMD system.

The collision force can be obtained from equation (1). c = the pounding damping, c can be obtained from equation (3). Here, δ = the viscoelastic material's deformation; $\dot{\delta}$ = the velocity of deformation; β = pounding stiffness coefficient; x_1 = displacements of the L-shaped steel beam;$\dot{x}_1$ = velocity of the L-shaped steel beam; x_2 = displacements of the delimiter; and $\dot{x}_2$ = velocity of the delimiter and g_p = distance between them.

$$u = \sqrt{\frac{h_1}{h_0}}, \tag{4}$$

where u = the restitution coefficient, which is related to the properties of viscoelastic materials. It can be calculated from experimental data. By freely dropping the ball towards the viscoelastic material, h_0 = the initial height and h_1 = rebound height, e can be calculated using equation (4).

2.3. Motion Equation of Bridge Structure Using PTMD under Earthquake Action.

$$[m_b]\{\ddot{x}_b\} + [c_p]\{\dot{x}_b\} + [k_b]\{x_b\} = -[m_b]\ddot{x}_g + \{F_p\}, \tag{5}$$

$$\begin{aligned} &\cdot \begin{pmatrix} m_b & \\ & m_p \end{pmatrix} \begin{Bmatrix} \ddot{x}_b \\ \ddot{x}_p \end{Bmatrix} + \begin{pmatrix} c_p & 0 \\ 0 & 0 \end{pmatrix} \begin{Bmatrix} \dot{x}_b \\ \dot{x}_p \end{Bmatrix} \\ &+ \begin{pmatrix} k_b + k_p & -k_p \\ -k_p & k_p \end{pmatrix} \begin{Bmatrix} x_b \\ x_p \end{Bmatrix} \\ &= -\begin{pmatrix} m_b & \\ & m_p \end{pmatrix} \begin{Bmatrix} 1 \\ 1 \end{Bmatrix} \ddot{x}_g + \begin{pmatrix} 1 \\ -1 \end{pmatrix} F_p. \end{aligned} \tag{6}$$

The structural diagram of using PTMD to control bridge vibration is shown in Figure 2. According to the collision force model in Section 2.2, equation (5) is the motion equation of bridge structure with PTMD under earthquake. The bridge structure and PTMD motion equation are shown in equation (6), where m = mass, c = damping, and k = stiffness and x = the displacement, $\dot{x}$ = velocity, and $\ddot{x}$ = the acceleration. Subscript "b" represents the bridge and "p" represents the PTMD. In equations (5) and (6), $\ddot{x}_g$ is the acceleration response caused by the earthquake and F_p is the collision force, which can be obtained by using equation (1).

2.4. Motion Equation of Bridge with PTMD under Vehicle Load

$$[m_b]\{\ddot{x}_b\} + [c_p]\{\dot{x}_b\} + [k_b]\{x_b\} = \{F_b + F_{b-p}\}, \tag{7}$$

$$[m_v]\{\ddot{x}_v\} + [c_v]\{\dot{x}_v\} + [k_v]\{x_v\} = \{F_G\} + \{F_{v-b}\}. \tag{8}$$

Equations (7) and (8) are matrices that provide the equations of motion for bridges and automobiles, respectively, where $[m]$ = mass matrice, $[c]$ = damping matrice, $[k]$ = stiffness matrice, $\{x\}$ = displacement, $\{\dot{x}\}$ = velocity, and $\{\ddot{x}\}$ = acceleration. The subscript "b" stands for the bridge and "v" stands for the vehicle. F = force, the subscript "b" denotes the external force acting on the bridge structure. "G" represents gravity, "$b-p$" represents the force generated by PTMD on the bridge, and "$v-p$" represents the vehicle-bridge interaction force.

$$m_p\ddot{x}_{pv}(t) + c_{pv}\dot{x}_{pv}(t) + k_{pv}x_{pv}(t) = -F^{v}_{p-b}(t) - HF^{vp}_{p-b}(t), \tag{9}$$

$$m_p\ddot{x}_{pl}(t) + c_{pl}\dot{x}_{pl}(t) + k_{pl}x_{pl}(t) = -F^{l}_{p-b}(t) - HF^{lp}_{p-b}(t), \tag{10}$$

$$m_p\{\ddot{X}_p\} + [c_p]\{\dot{X}_p\} + [K_p]\{X_p\} = \{F_{p-b}\} + RT\{F^{p}_{p-b}\}. \tag{11}$$

Equations (9)–(11) represent the equations of motion for the PTMD-bridge interaction [36], where m = mass, c = damping, and k = stiffness. The subscript "p" stands for PTMD, "v" stands for the vertical direction, and "l" stands for lateral direction. $F_{p-b}(t)$ = force of interaction between PTMD and bridge and F^{p}_{p-b} = pounding forces. Superscript "l" stands for the lateral direction and "v" stands for the vertical direction. F^{p}_{p-b} can be computed by using equation (1), R = direction of the pounding force, and T = location of the pounding forces.

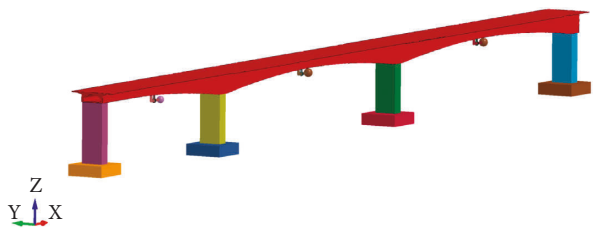

Figure 2: bridge model with PTMD.

$$\begin{pmatrix} m_b & & \\ & m_p & \\ & & m_v \end{pmatrix} \left\{ \ddot{X}_b \ddot{X}_p \ddot{X}_v \right\} + \begin{pmatrix} C_b + C_b^v + C_b^p & C_{b-p} & C_{b-v} \\ C_{p-b} & C_p + C_{p-p} & 0 \\ C_{v-b} & 0 & C_v \end{pmatrix} \begin{Bmatrix} \dot{X}_b \\ \dot{X}_p \\ \dot{X}_v \end{Bmatrix} + \begin{pmatrix} K_b + K_b^v + K_b^p & K_{b-p} & K_{b-v} \\ K_{p-b} & K_p + K_{p-p} & 0 \\ K_{v-b} & 0 & K_v \end{pmatrix} \begin{Bmatrix} X_b \\ X_p \\ X_v \end{Bmatrix} = \begin{Bmatrix} F_{b-r} + F_{b-p} \\ F_{p-b} + RTF_{p-b}^p \\ -F_{v-r} + F_G \end{Bmatrix}. \quad (12)$$

Through the aforementioned analysis, combined with the vehicle-bridge motion equation, equation (12) illustrates the PTMD-vehicle-bridge system's equation of motion [36, 46], where m = mass, c = damping, and k = stiffness; subscripts "b," "p," and "v" denote the bridge, PTMD, and vehicles, respectively; superscripts "p" and "v" represent contributions from PTMD and vehicles, respectively; subscripts "$b-v$" and "$v-b$" denote the vehicle-bridge interaction. F_{b-r} = the force formed by the uneven road surface on the bridge structure; F_{v-r} = the force formed by the uneven road surface on the vehicles; and F_G = the gravity of the vehicle.

3. The Numerical Analysis Model

3.1. Bridge Prototype. The prototype bridge (Figure 3) is a three-span continuous structure with an effective span of 120 m + 120 m + 80 m. The upper structure is composed of a variable cross-section prestressed concrete box girder. A cross-sectional view of the bridge midspan and the top of the pier is shown in Figure 4. The piers are hollow box piers.

The bridge's midspan exhibits the most displacement along the direction of seismic excitations movement. Therefore, the positions of these three PTMDs are all placed in the middle of the three spans.

3.2. Bridge's Multiscale Finite Element Model. Figure 5 illustrates the numerical model created with LS-DYNA, which shows the numerical calculation model of the prototype bridge and each component. The entire structure is divided into bridge piers, caps, concrete box girder, and PTMD, Figures 5(a)–5(c) represent the bridge deck, piers, caps, and PTMD, respectively. The concrete box girder is made up of solid elements; the bridge piers and caps adopt beam elements, the PTMD limiter and mass block adopt solid elements, and the L-shaped steel beam adopts beam elements. There are 94,830 solid elements and 341 beam elements in the total model. Among them, the concrete box girder has 89380 units, the bridge piers and caps have 226 units, and the PTMD has 5565 units. The boundary conditions are set as follows. The bottom surfaces of caps are consolidated, and horizontal and vertical constraints are added at the connections between the bridge's upper structure and the piers. Moreover, the nodes at the junctions of the piers and the caps adopt consolidation constraints. One end of the L-shaped steel beam is connected with the mass block and the other end is consolidated with the bridge superstructure.

C 55 concrete is used for variable section box girders; the bridge piers and caps are made of C 40 concrete. Both the limiter of the PTMD and L-shaped rod are made out of steel, and the limiter is attached with viscoelastic material. The material parameters of C 40 concrete are the following: $E_1 = 32500$ MPa, $\mu_1 = 0.2$, $G_1 = 13000$ MPa, $f_{c1} = 18.4$ MPa, and $f_{t1} = 1.65$ MPa; and the material parameters of C50 concrete include the following: $E_2 = 32500$ MPa, $\mu_2 = 0.2$, $G_2 = 13000$ MPa, $f_{c2} = 18.4$ MPa, and $f_{t2} = 1.65$ MPa. PTMD is composed of steel and viscoelastic material, their main parameters are $\rho_1 = 7850\ \text{kg/m}^3$, $E_1 = 200000$ MPa, $\mu_1 = 0.3$, $\rho_2 = 1150\ \text{kg/m}^3$, $E_2 = 2000$ MPa, and $G = 0.6$ MPa, respectively. Among them, E = the elastic modulus, μ = Poisson's ratio, G = the shear modulus, ρ = density, f_c = concrete compressive strength, and f_t = the tensile strength of concrete.

3.3. Vehicles' Finite Element Model. This study uses Ford's simplified model (21724 elements) single-unit truck (SUT) (Figure 6) as the vehicle load. The truck model can be downloaded from the NCAC website. The accuracy of each model is verified through frontal collision experiments [37]. Both models highly correlated with experimental results. The entire vehicle modulus consists of 21,724 elements, including 123 beam elements, 20,109 shell elements, and 1,492 solid elements.

3.4. Modal Analysis of the Bridges. Using the finite element model in 3.2 for modal analysis, the first two-order frequencies and mode shape descriptions of the bridge are shown in Table 1, and the formation diagram is shown in Figure 7.

The bridge's lateral angular frequency in the absence of a control is $\omega_1 = 12.3$ rad/s and $\omega_2 = 22.3$ rad/s. In addition, $\xi = 0.05$, when the values are substituted in Rayleigh's formula, it produces the following results $a = 0.79$ and $b = 0.003$, and with PTMD installed, we get $a = 0.64$ and $b = 0.004$. Similar to this, the bridge's vertical calculation results are the following: without any control, $a = 0.57$ and $b = 0.004$; and with PTMD installed, $a = 0.48$ and $b = 0.005$. The numerical computations that follow will make use of the results.

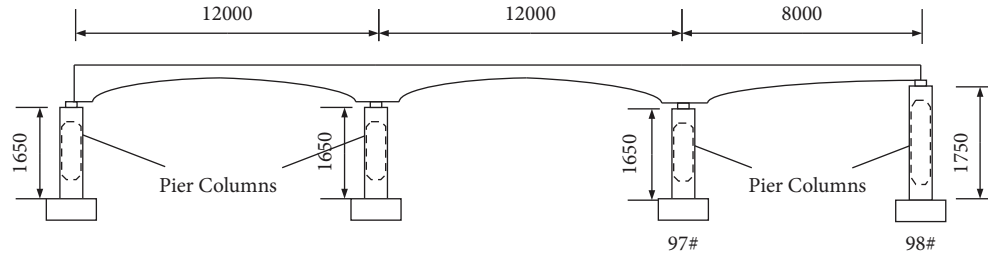

Figure 3: Elevation of a three-span continuous bridge (unit: cm).

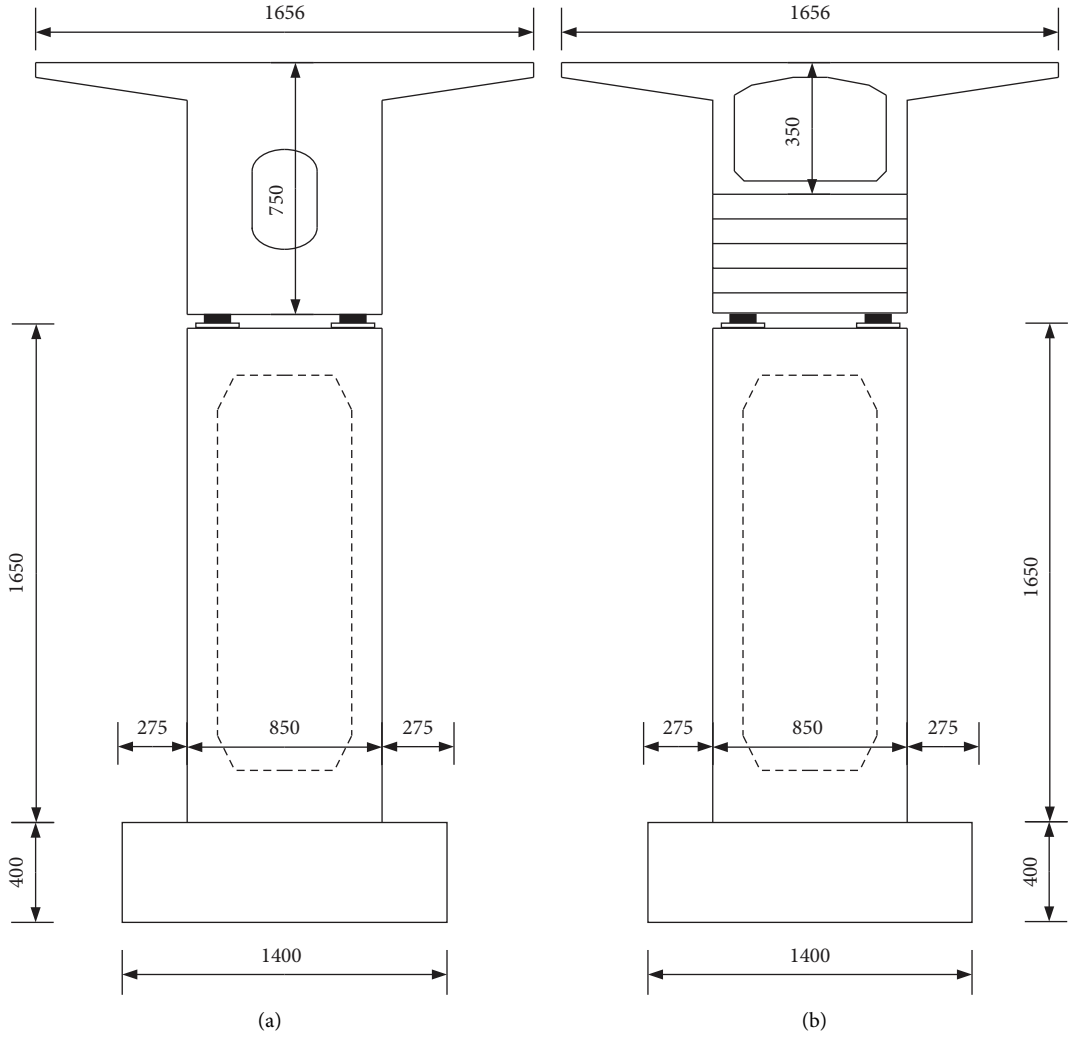

Figure 4: Transverse views of the bridge (unit: cm): (a) cross-section of the top of the pier and (b) cross-section at the midpoint of the span.

4. Optimization of PTMD Parameters

The bridge's location is relatively weak in seismic activity and the site category is Category III. The record from the El-Centro earthquake (suitable for Category II and III sites) is selected as the seismic excitation. Figure 8 depicts t as the acceleration time histories of the record from El-Centro, with a hight of 0.4 g.

4.1. Initial Determination of PTMD Parameters. Figure 9 shows the various parameters of PTMD and Table 2 lists their precise values. The parameters of PTMD affect the vibration reduction effect of PTMD so that it can be optimized for the main parameters.

Where g_p = the collision gap.

$$\lambda = \frac{L_1}{L}, \tag{13}$$

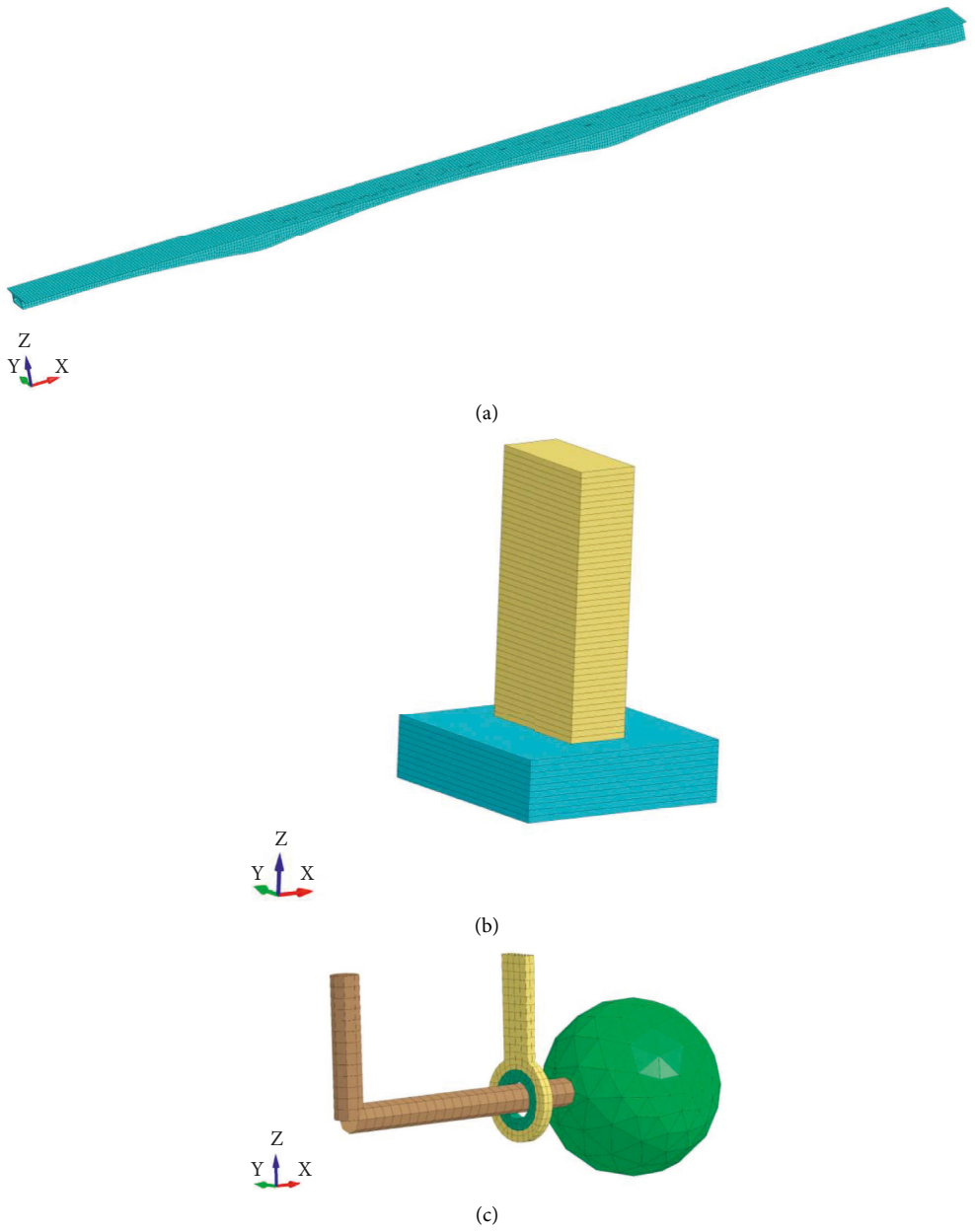

Figure 5: The finite element model of the bridge: (a) main beam, (b) pier columns and caps, and (c) PTMDs.

where λ = length ratio.

$$g_p = R_1 - R_4, \tag{14}$$

The mass ratio u is defined by

$$u = \frac{m}{M_b}, \tag{15}$$

where u = mass ratio, m = the mass block's mass, and M_b = the mass of the superstructure of the bridge span where the PTMD is located. We use the damping rate to evaluate the damping effect of the damper.

$$\mu = \frac{D - D_C}{D} \times 100\%. \tag{16}$$

In the formula, D represents the displacement peak without PTMD, D_C represents the displacement peak value of the PTMD damping device installed, and μ represents the damping rate.

4.2. The Effect of Length Ratio. λ is an important parameter of PTMD, which determines the installation position of the L-shaped steel beam and also affects the vibration reduction effect of PTMD. The length ratio of 0.2–0.7 is selected for optimal design, and Figure 10 displays the vibration reduction rate's fluctuation curve with λ. When the length ratio of the three spans is 0.6, the vibration reduction rate is the highest. The vibration reduction rate of the 80-meter side

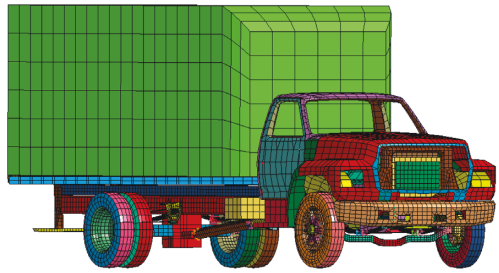

Figure 6: The finite element model of the truck.

Table 1: The first two modal analysis results of the bridge.

Mode shape	Frequency, f (Hz)		Angular frequency, ω (rad/s)		Period (s)	
	Uncontrolled	With PTMD	Uncontrolled	With PTMD	Uncontrolled	With PTMD
First-order cross bend	1.96	1.65	12.3	10.4	0.5	0.6
Second-order cross bend	3.55	2.69	22.3	16.9	0.3	0.4
First-order vertical bend	1.69	1.35	10.6	8.5	0.6	0.7
Second-order vertical bend	1.93	1.75	12.1	11.0	0.5	0.6

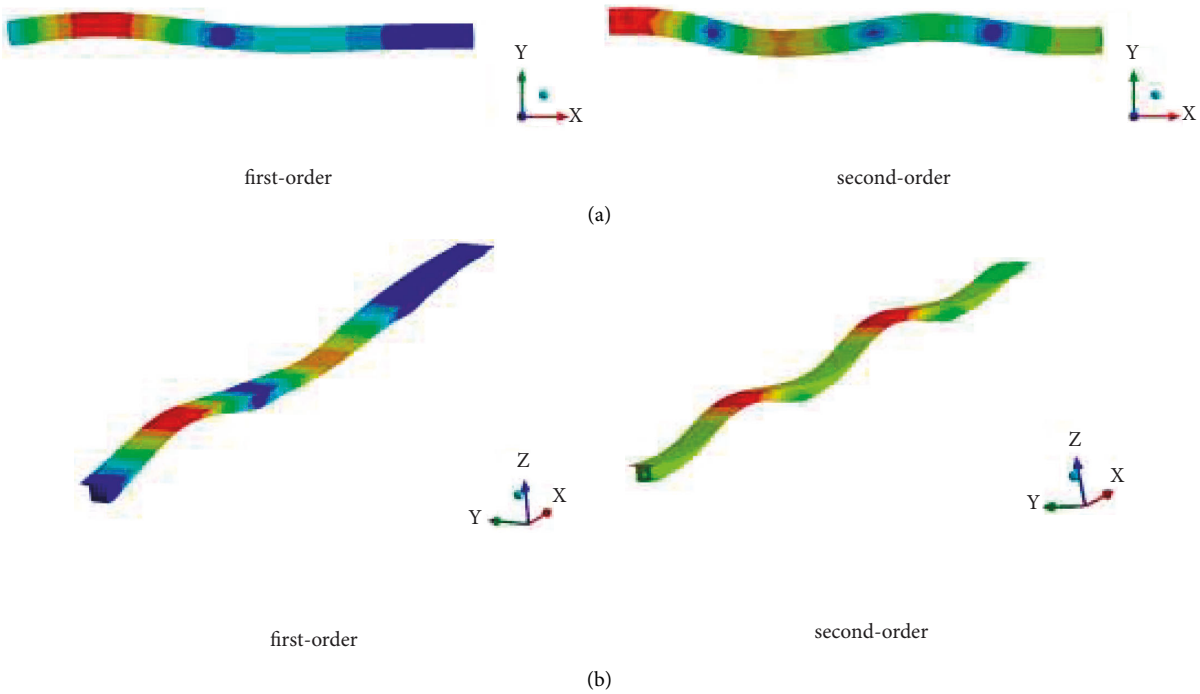

Figure 7: Bridge mode shapes: (a) lateral: X direction; and (b) vertical: Z direction.

span, the 120-meter midspan, and the 120-meter side span reaches 15.1%, 44.6%, and 28.5%, respectively.

4.3. Length Ratio Impact. The vertical length is an important parameter of PTMD. The vertical length of 2 meters, 2.5 meters, and 3.5 meters was selected for comparative analysis. The length ratio λ is 0.6, and other parameters of PTMD are still the same as shown in Table 2. The vibration reduction rate is best when H_1 is 2 meters, as shown in Table 3 and Figure 11. This is because, the shorter the vertical length, the closer the collision site is to the main beam, and the more noticeable is the reduction in the dynamic response to the bridge structure.

Among them, when the vertical length is 2.5 meters, the shock absorption effect of PTMD is not much different from that of 2 meters. Simultaneously, a vertical length of 2.5 m is chosen to prevent PTMD's vertical vibration from colliding with the bridge's superstructure. In the actual project, the value of H_1 should be comprehensively considered according to the installation space and the vibration amplitude.

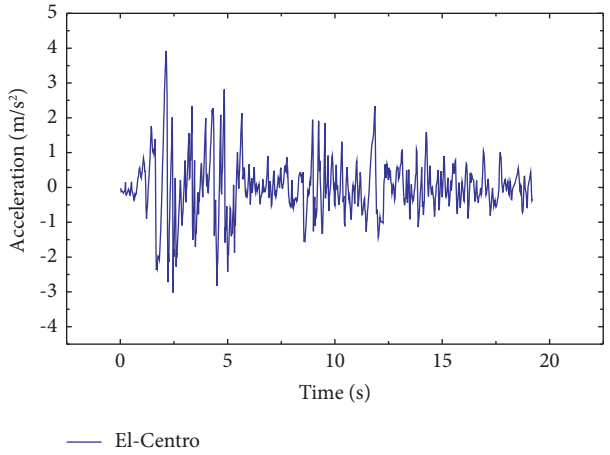

Figure 8: Acceleration time histories of the record from the El-Centro earthquake.

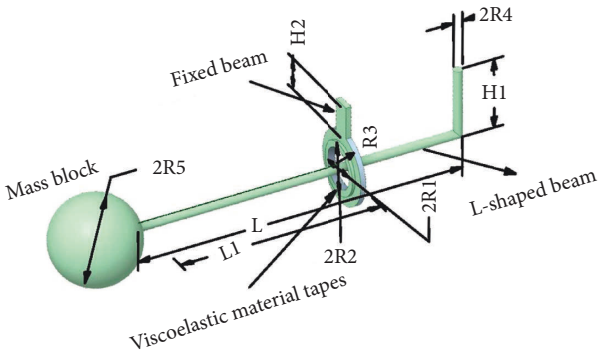

Figure 9: A schematic diagram of PTMD parameters.

Table 2: Parameters of PTMD.

Span (m)	The mass ratio (%)	Quality (t)	H_1 (m)	L (m)	R_1 (cm)	R_2 (cm)	R_3 (cm)	R_4 (cm)
120	2	121.2	2.5	5	33	53	73	25
80	2	67.8	2.5	5	33	53	73	25

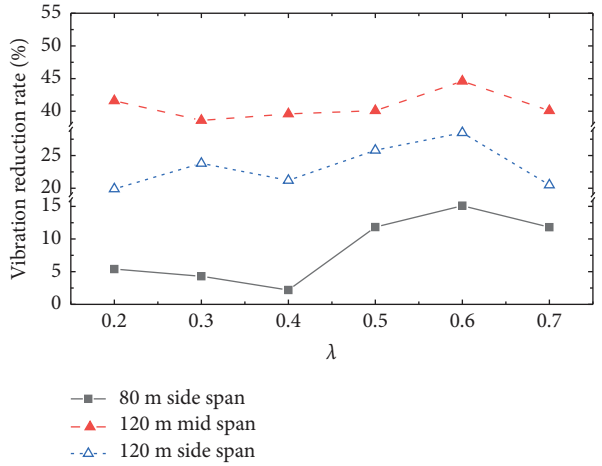

Figure 10: Vibration reduction ratios with various length ratios.

Table 3: Dynamic responses of bridges with different PTMDs.

Span (m)	H1 (m)	Displacement (m)	Displacement of uncontrolled bridges (mm)	Vibration reduction rate
80	2	78	93	16.1
	2.5	80	93	14.0
	3.5	83	93	10.8
120 (midspan)	2	110	202	45.6
	2.5	112	202	44.6
	3.5	120	202	40.6
120 (side span)	2	112	151	25.8
	2.5	112	151	25.8
	3.5	116	151	23.2

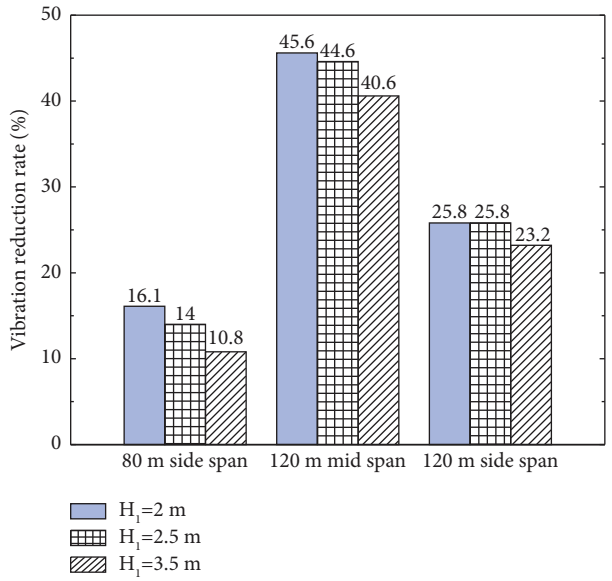

Figure 11: A parametric study of vertical length on the vibration reduction rate.

Table 4: Parameters of PTMD with different collision gaps.

Span (m)	U (%)	m (t)	H_1 (m)	L (m)	R_1 (cm)	R_2 (cm)	R_3 (cm)	R_4 (cm)	g_p (cm)
120	2	121.2	2.5	5	31	51	71	25	6
					33	53	73	25	8
					35	55	75	25	10
					37	57	77	25	12
80	2	67.8	2.5	5	31	51	71	25	6
					33	53	73	25	8
					35	55	75	25	10
					37	57	77	25	12

Table 5: Comparison of PTMD vibration reduction effects under different collision gaps.

Span (m)	Collision gap (cm)	Displacement peak (mm)	The vibration reduction rate (%)	Speed peak	The vibration reduction rate (%)
80	No control	93	—	0.85	—
	6	80	14.0	0.61	28.2
	8	79	15.1	0.61	28.2
	10	79	15.1	0.6	29.4
	12	82	11.8	0.63	25.9
120 (midspan)	No control	202	—	1.51	—
	6	117	42.1	1.02	32.5
	8	112	44.6	0.96	36.4
	10	110	45.5	1.0	33.8
	12	119	41.1	1.02	32.5

Table 5: Continued.

Span (m)	Collision gap (cm)	Displacement peak (mm)	The vibration reduction rate (%)	Speed peak	The vibration reduction rate (%)
	No control	151	—	1.19	—
	6	114	24.5	0.83	30.3
120 (side span)	8	108	28.5	0.74	37.8
	10	115	23.8	0.77	35.3
	12	120	20.5	0.9	24.4

Table 6: PTMDs' parameters with various mass ratios.

Span (m)	U (%)	m (t)	H_1	L_1	L	L_1/L	Collision gap (cm)
120	1	80.8	2.5	3	5	0.6	8
	1.5	121.2	2.5	3	5	0.6	8
	2	161.6	2.5	3	5	0.6	8
80	1	45.2	2.5	3	5	0.6	8
	1.5	67.8	2.5	3	5	0.6	8
	2	90.5	2.5	3	5	0.6	8

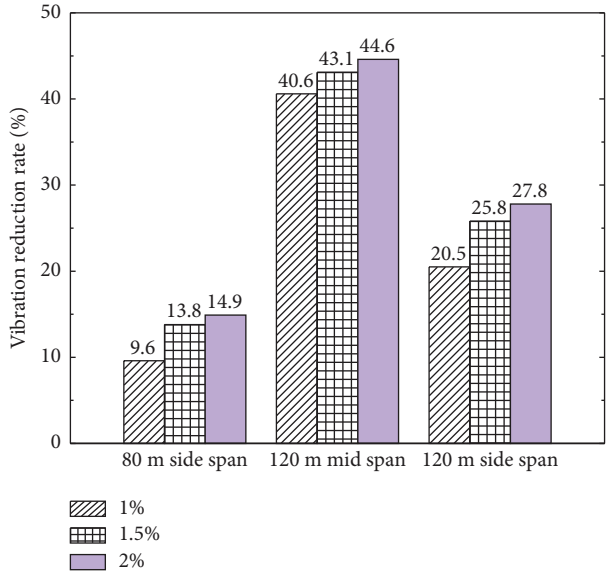

Figure 12: A parametric study of mass ratio on the vibration reduction rate.

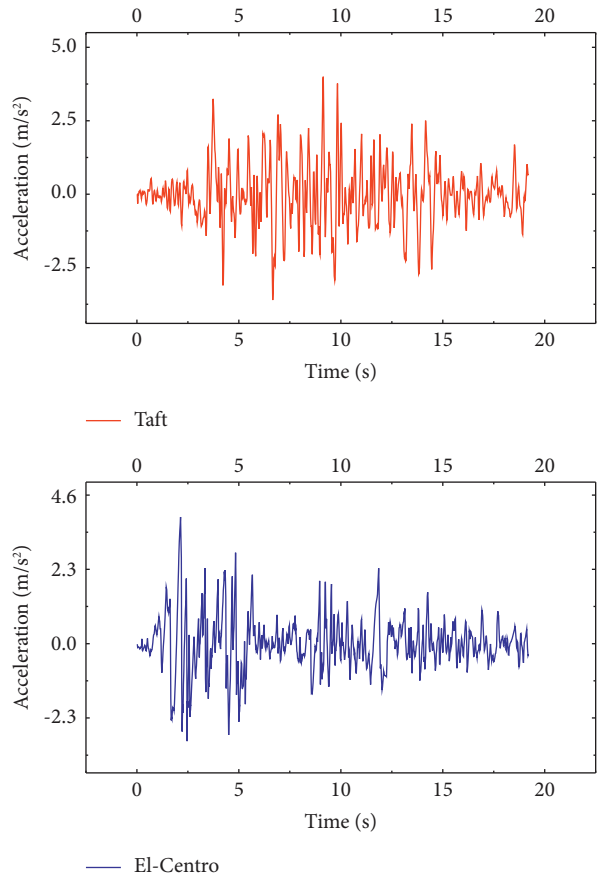

Figure 13: Acceleration time histories of the two records from the El-Centro and Taft earthquakes.

Table 7: Parameters of PTMDs.

Span (m)	u (%)	m (t)	H_1	L_1	L	L_1/L	Collision gap (cm)
120	1.5	121.2	2.5	3	5	0.6	8
80	1.5	67.8	2.5	3	5	0.6	8

4.4. Impact of Collision Gap. The collision gap refers to the distance between the L-shaped steel beam and the viscoelastic material. The size of the collision gap determines the speed of the steel beam before the collision and determines the deformation of the viscoelastic material. In this section, four kinds of collision gaps, 6 cm, 8 cm, 10 cm, and 12 cm, are selected for comparative analysis. Besides, the impact of various collision gaps on the PTMD's vibration control effect is investigated. Table 4 shows the PTMD's unique specifications, and Table 5 displays the bridge-PTMD system's dynamic reaction for various collision gaps. Considering the dynamic response of the three spans, the most suitable collision gap is 8 cm.

Table 8: Seismic response of the bridge under the record from the El-Centro earthquake with and without PTMD.

Span (m)	Structural response	Peak value		Decrease rate
		No control	PTMD	
120 (side span)	Displacement (m)	0.151	0.112	25.8%
	Velocity (m/s)	1.2	0.74	38.3%
120 (midspan)	Displacement (m)	0.202	0.115	43.1
	Velocity (m/s)	1.5	1.0	33.3
80	Displacement (m)	0.93	0.81	12.9
	Velocity (m/s)	0.85	0.60	29.4

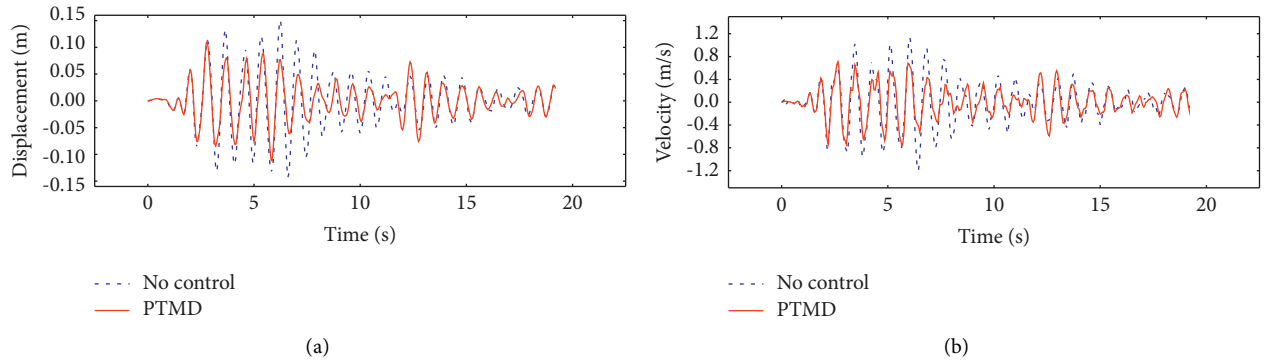

Figure 14: Dynamic response of 120-m side span under the record from the El-Centro earthquake: (a) displacement and (b) velocity.

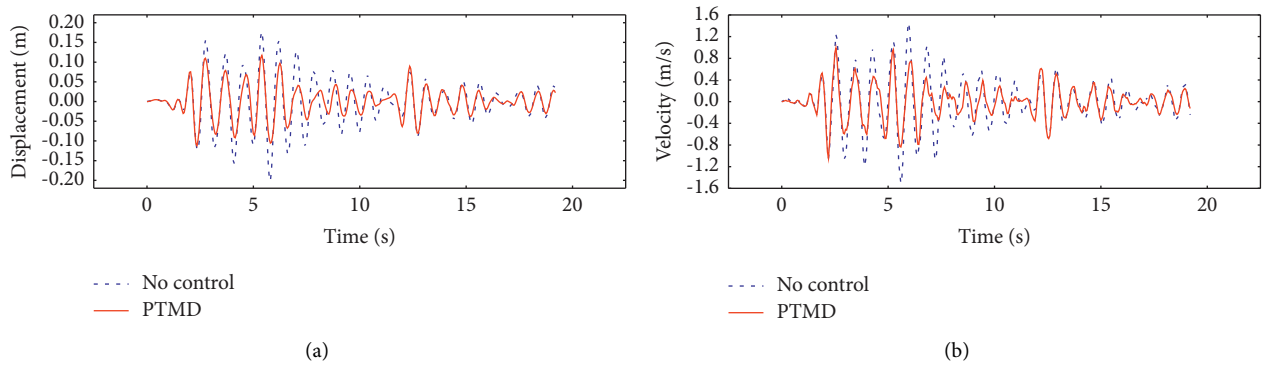

Figure 15: Dynamic response of 120-m midspan under the record from the El-Centro earthquake: (a) displacement and (b) velocity.

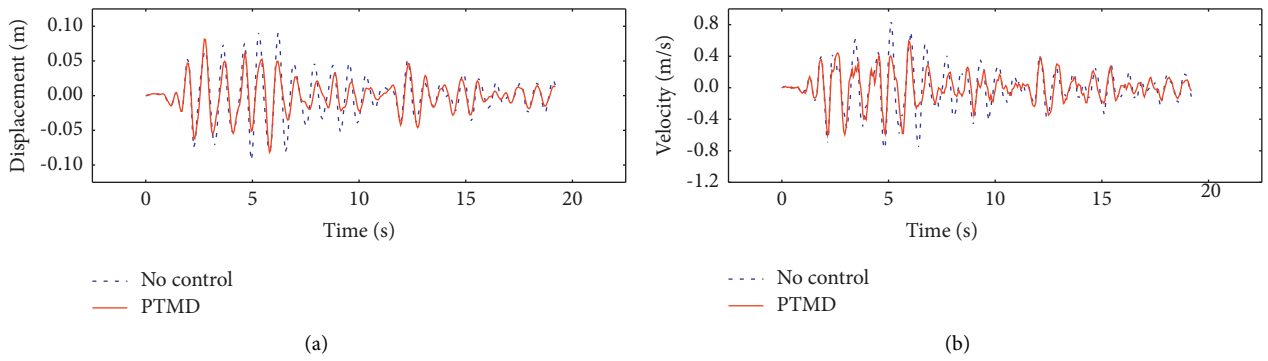

Figure 16: Dynamic response of 80-m side span under the record from the El-Centro earthquake: (a) displacement and (b) velocity.

4.5. The Effect of Mass Ratio. The mass ratio (u) is an important parameter of PTMD. Three distinct values of mass ratio, 1.0%, 1.5%, and 2.0%, were chosen for computation in order to evaluate the impact of mass ratio on the vibration reduction effect of PTMD. To evaluate its damping performance, the reduction rate of the three-span midspan node's lateral displacement and velocity is used. The design parameters of PTMD under four mass ratio conditions are shown in Table 6.

Figure 12 depicts the vibration reduction rate of PTMD at various mass ratios, the vibration reduction rate is greatest at the mass ratio of 2%. 80-meter side span, 120-meter midspan, and 120-meter side span, all have vibration reduction rates of 14.9%, 27.8%, and 44.6%, respectively. The mass ratio of 1.5 percent has a slightly less than two percent impact on vibration reduction. However, the vibration reduction rate of 1% is greatly decreased. A complete analysis reveals that the mass ratio of 1.5% is ideal for reducing the bulk of the mass ball and preventing the midspan stress concentration.

Through the analysis of 4.1~4.5, the optimized PTMD parameters for bridge vibration control are shown in Table 7.

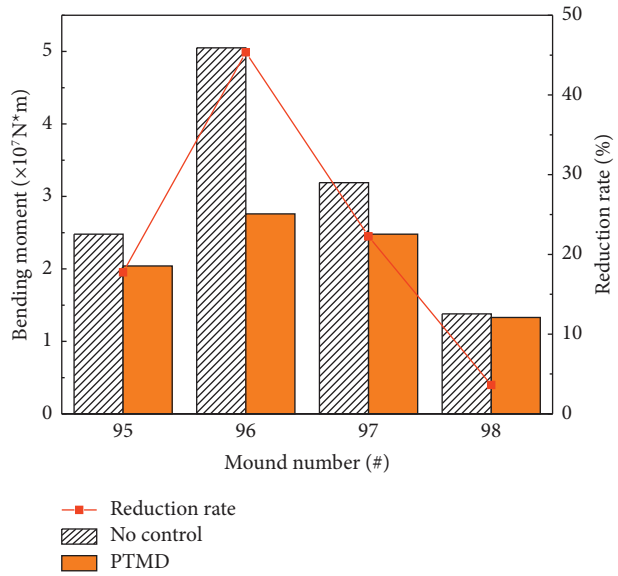

Figure 17: Bending moment around the longitudinal bridge at the base of the pier.

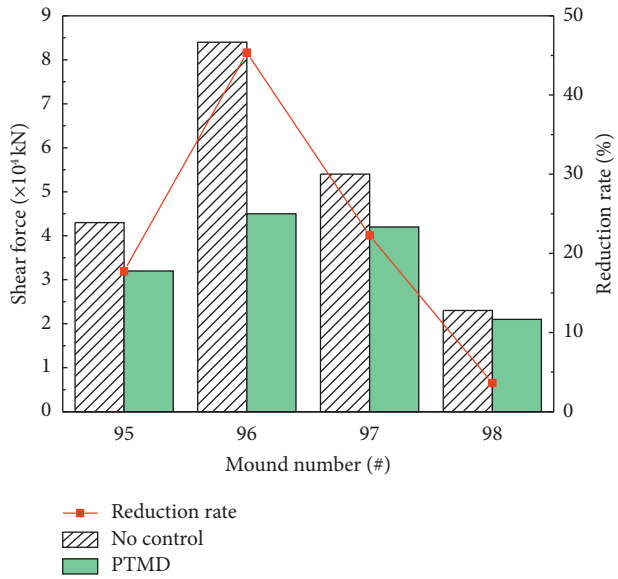

Figure 18: Transverse shear force at the pier bottom.

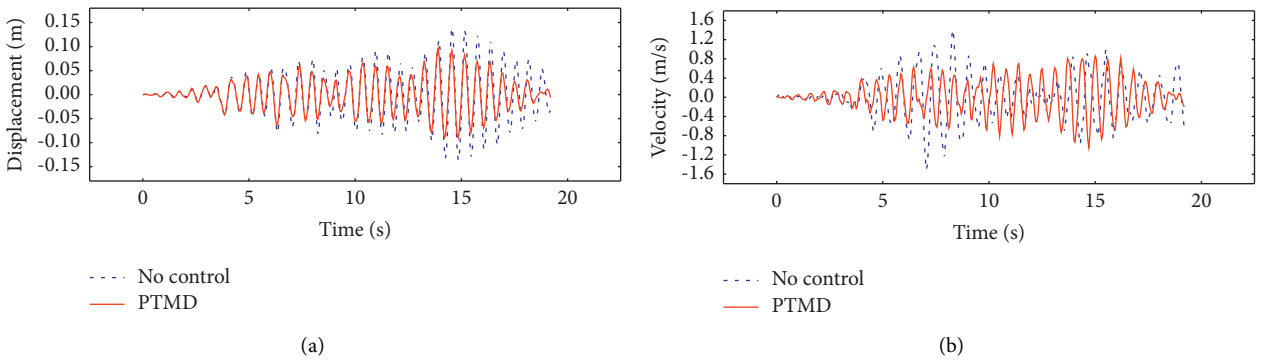

Figure 19: Dynamic response of 120-m side span under the record from the Taft earthquake: (a) displacement and (b) velocity.

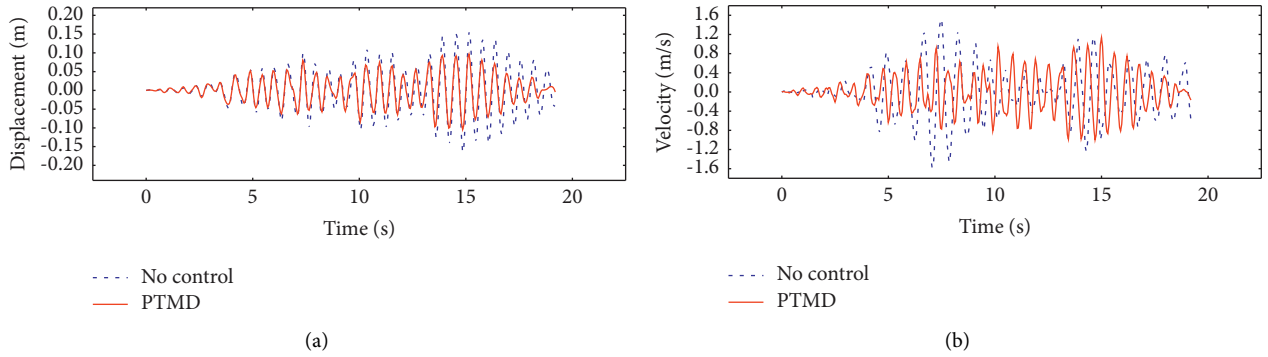

Figure 20: Dynamic response of 120-m midspan under the record from Taft earthquake: (a) displacement and (b) velocity.

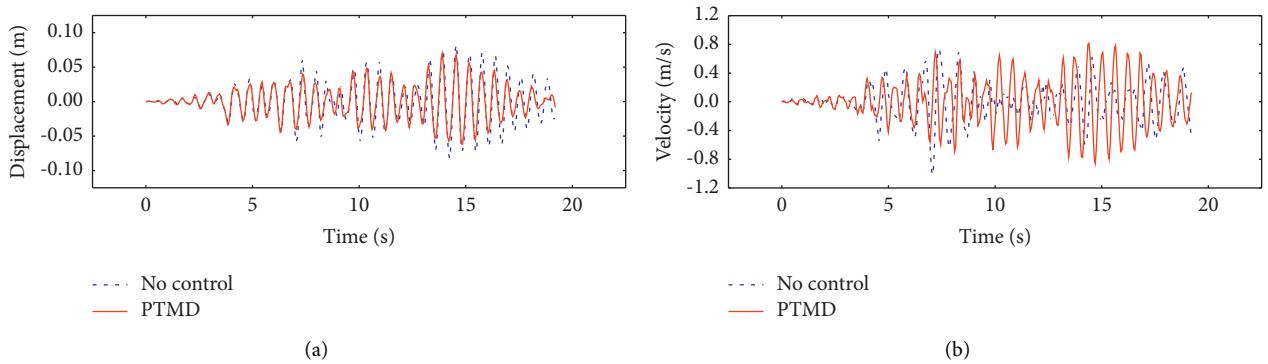

Figure 21: Dynamic response of 80-m side span under the record from the Taft earthquake: (a) displacement and (b) velocity.

Table 9: Seismic response of the bridge under the record from the Taft earthquake with and without PTMD.

Span (m)	Structural response	Peak value		Decrease rate (%)
		No control	PTMD	
120 (side span)	Displacement (m)	0.139	0.096	30.9
	Velocity (m/s)	1.56	1.04	33.3
120 (midspan)	Displacement (m)	0.165	0.104	37.0
	Velocity (m/s)	1.7	1.13	33.5
80	Displacement (m)	0.082	0.07	14.6
	Velocity (m/s)	0.85	0.78	8.2

5. Result Analysis

5.1. The Transverse Bridge Vibration Reduction Effect of PTMD under Earthquakes. Two recorded ground motions from the El-Centro (0.4 g) and Taft (0.4 g) earthquakes, were utilized for transverse direction excitation. A time history study was subsequently completed to confirm the effect of PTMD on lateral vibration control of the bridge. Figure 13 displays the acceleration time histories of two recordings.

5.1.1. Excitation of the Record from the El-Centro Earthquake

(1) Displacement and Velocity of Midspan Nodes. The record from the El-Centro earthquake was chosen as a seismic stimulation. The bridge's seismic reaction is displayed in Table 8 both with and without the PTMD. Figures 14–16 display the dynamic response (velocities and displacements at midspan) of the bridge for three spans. The picture demonstrates how useful it might be to employ PTMD to lessen the peak velocity and displacement at midspan. The uncontrolled bridge's 120-meter side span, 120-meter center span, and 80-meter side span all have peak displacements of 0.151 m, 0.202 m, and 0.93 m, respectively. The peak displacement values were lowered to 0.112 m, 0.115 m, and 0.81 m after the installation of the PTMD control device, with corresponding reduction rates of 25.8%, 43.1%, and 12.9%.

(2) Bending Moment of Pier Bottom. There are a variety of explanations for bridge damage induced by earthquakes, one of which is bridge pier damage caused by high bending moments at the piers' bottoms. The bending moment of the pier bottom around the longitudinal bridge is much greater

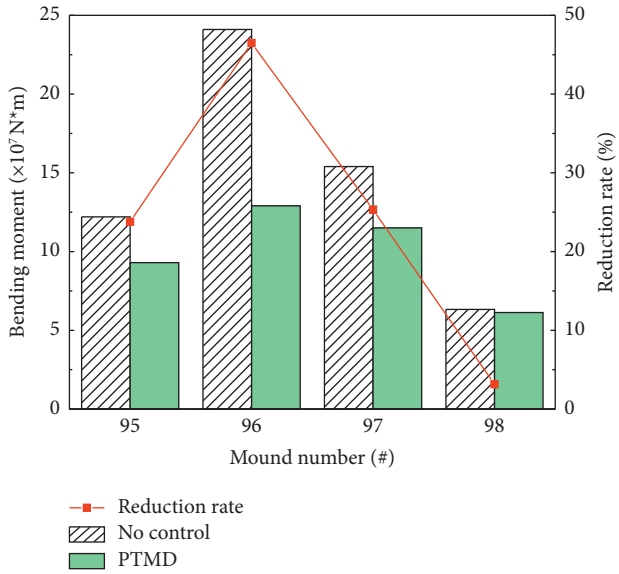

Figure 22: Bending moment around the longitudinal bridge at the base of the pier.

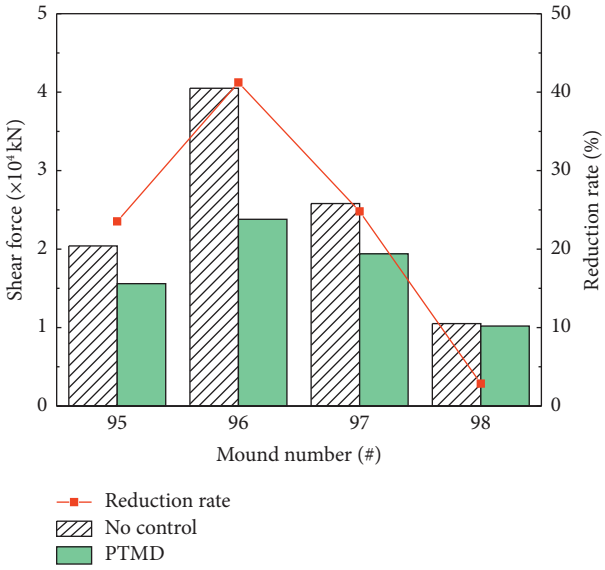

Figure 23: Transverse shear force at the pier bottom.

than that around the transverse bridge due to the transverse loading of seismic excitations. Figure 17 depicts, both without control and using PTMD, the maximum longitudinal bending moment at the bottom of the bridge's pier. As shown in Figure 17, piers 96 and 97 have the best bending moment reduction effect, reaching 45% and 22%, respectively. In addition, the maximum bending moments of the remaining piers also were reduced. Therefore, it is clear that the PTMD device may increase the seismic performance of the bridge while also reducing the bending moment at the base of the pier.

(3) Shear Force at the Bottom of the Pier. Shear force is a major cause of bridge damage caused by earthquakes. Figure 18 depicts the maximum shear force at the bottom of bridge piers with and without PTMD. As can be seen in the diagram, PTMD may effectively lower the shear force at the bridge pier's bottom. Among them, the shear force of No. 96 pier has the most obvious reduction effect, which is reduced by 46%. The shear force of the other piers has been significantly reduced as well. PTMD may greatly reduce shear stress at the bottom of bridge piers, as well as earthquake-related damage to bridge piers.

5.1.2. Excitation of the Record from the Taft Earthquake

(1) Displacement and Velocity of Midspan Nodes. The Taft ($0.4g$) earthquake record is used as the source of seismic excitation. The lateral displacement and velocity time-history curve of the three-span midspan node of the main bridge are shown in Figures 19–21. Besides, the seismic response comparison of bridges with and without the PTMD system under the record from the Taft earthquake is shown in Table 9. The findings suggest that PTMD can successfully minimize the maximum velocity and displacement in the midspan. The peak displacements of the 120-m side span, 120-m midspan, and 80-m side span of the uncontrolled bridge are 0.139 m, 0.165 m, and 0.082 m, respectively. After installing the PTMD control device, the peak midspan displacement was reduced to 0.096 m, 0.15 m, and 0.1 m, respectively, and the reduction rates were 30.9%, 37%, and 14.6%, respectively. It is clear that PTMD can lessen bridge reaction during the excitation of the record from the Taft earthquake.

(2) Bending Moment of Pier Bottom. Figure 22 illustrates the maximum bending moment at the pier bottom with and without PTMD control around the longitudinal bridge. Piers 96 and 97 exhibit the highest pier bottom bending moments, which were decreased by 46.5% and 25.3%,

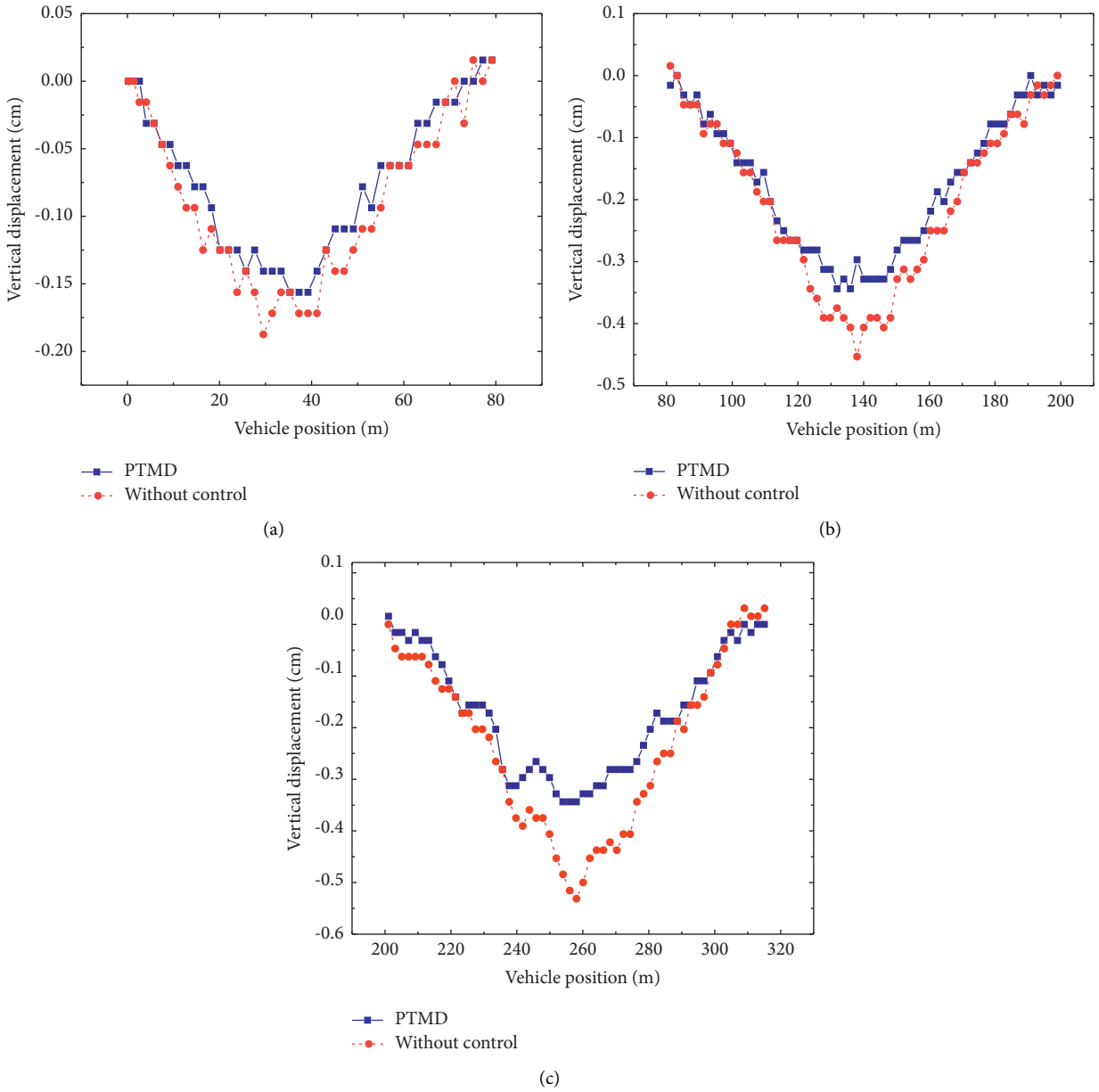

Figure 24: The dynamic displacement of the three-span bridge under the truck movement: (a) side span (80 m), (b) midspan (120 m), and (c) side span (120 m).

Table 10: Response of bridges without and with PTMD.

Span (m)	Structural response	Peak value		Decrease rate (%)
		No control	PTMD	
80 (side span)	Midspan displacement (cm)	−0.19	−0.16	15.8
120 (midspan)	Midspan displacement (cm)	−0.45	−0.34	24.4
120 (side span)	Midspan displacement (cm)	−0.53	−0.34	35.8

respectively, once PTMD devices were installed. Consequently, the PTMD device can decrease bridge piers' bending moment caused by the recorded ground motion from the Taft earthquake and can improve the safety of the bridge.

(3) Shear force at the bottom of the pier. Figure 23 displays the maximum shear force of the bridge's four piers both with and without PTMD. It is obvious that PTMD can greatly lessen the shear stress at the bridge pier's bottom. No. 96's pier bottom shear force has been reduced by 41.2%, and that

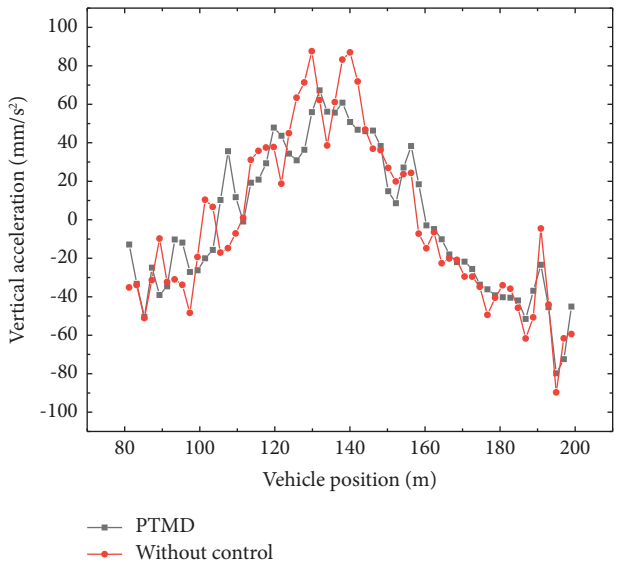

Figure 25: Acceleration of a single vehicle moving on midspan (120 m) of the bridge.

of the other bridge piers has also been significantly reduced. The bridge piers' shear force may be greatly lowered by using PTMD, which lessens the earthquake's damage to the pier.

5.2. Analysis of the Vertical Vibration Reduction Effect of PTMD under Vehicle Load

5.2.1. Comparison of Bridge Vibration with or without PTMD under Vehicle Load. The vehicle in this research is traveling at an average speed of 80 km/h on the bridge. Figure 24 plots the dynamic deflection time history of a three-span bridge without a vibration suppression system and with a PTMD system. Figure 24 shows how PTMD may minimize the vertical displacement of the bridge structure greatly. For example, the maximum midspan displacement of a 120 m long bridge without control and with PTMD control is 0.37 cm and 0.31 cm, respectively, and the reduction rate is 13.9%. As shown in Table 10, the midspan displacement of the other two spans of 80 m and 120 m of the bridge with the PTMD system decreased by 15.8% and 35.8%, respectively. As a result, the PTMD system may significantly minimize the bridge's vertical vibration caused by vehicle loads.

5.2.2. Comparison of Car Driving Comfort. For the driver, the change of acceleration directly reflects the driving comfort and reflects the vibration of the vehicle. Due to the large difference in the acceleration of each node of the vehicle, the vehicle engine as a whole is selected as the research object. When the vehicle travels to the midspan of 120 meters, its vertical acceleration varies with the position of the vehicle, as shown in Figure 25. PTMD is particularly successful in reducing the vehicle's vertical acceleration. In Figure 25, the peak acceleration of the vehicle without the control system is 0.087 m/s^2, while the peak acceleration of the midspan node of the PTMD bridge is 0.051 m/s^2. Acceleration was reduced by 41.4%. The vertical vibration of the bridge structure may be reduced using PTMD, which reduces vehicle vibration and improves driving comfort.

6. Conclusion

PTMD is employed in this work to regulate earthquake-induced lateral transverse bridge vibrations as well as vertical vehicle-induced vibrations. The motion equations of the bridge-PTMD system under earthquake and the vehicle-bridge-PTMD system are established, and parameters are optimized for PTMD. Furthermore, numerical analysis is carried out under different seismic excitations and vehicle loads. Numerical simulations show the following:

(1) In this study, length ratio, vertical length, collision gap, and mass ratio are selected as design parameters. Subsequently, the parameters are optimized by numerical simulation, and PTMDs' vibration reduction impact is improved.

(2) Under the impact of an earthquake, the vibration of the bridge in its transverse direction can be significantly reduced using the PTMD. The PTMD may effectively minimize bridge seismic response, as well as the midspan node velocity, displacement, shear force, and bending moment of the pier bottom. Therefore, the PTMD improves the bridge's seismic performance.

(3) Based on the PTMD system of a three-span bridge under the action of a single vehicle, the PTMD can lower the vertical vibration amplitude of the bridge, according to numerical estimates. The displacement of the 80-m side span, 120-m midspan, and 120-m side span of the bridge with PTMDs system decreased by 15.8%, 24.4%, and 35.8% respectively. The PTMD technology lessens the vehicle's vertical acceleration, lessens its vibration, and enhances driving comfort.

In this study, the PTMD is applied to the vibration control of large-span continuous girder bridges, and the numerical simulations have obtained very good results. But there are still some problems that need to be further studied and improved, mainly in the following aspects:

(1) In order to further study the vibration control effect of PTMD, the PTMD system can be fabricated and installed on a scale bridge to study its vibration control effect.

(2) Under the action of random traffic flow, the dynamic response of bridges with or without PTMD needs further study.

Data Availability

The data supporting the current study are given in the article.

Conflicts of Interest

The authors declare that they have no conflicts of interest.

Acknowledgments

The authors would like to thank the National Natural Science Foundation of China: No. 52079128; and Science and Technology Project of Henan Province, No. 212102310289, for their support.

References

[1] W. Guo, Y. Hu, H. Liu, and D. Bu, "Seismic performance evaluation of typical piers of China's high-speed railway bridge line using pushover analysis," *Mathematical Problems in Engineering*, Advance online publication, vol. 2019, , 2019.

[2] X.-X. Liu and Y. Wang, "A novel seismic risk analysis method for structures with both random and convex set mixed variables: case study of a RC bridge," *Mathematical Problems in Engineering*, Advance online publication, vol. 2019, , 2019.

[3] K. Meng, C. Cui, Z. Liang, H. Li, and H. Pei, "A new approach for longitudinal vibration of a large-diameter floating pipe pile in visco-elastic soil considering the three-dimensional wave effects," *Computers and Geotechnics*, vol. 128, Article ID 103840, 2020.

[4] K. Meng, C. Cui, and H. Li, "An ontology framework for pile integrity evaluation based on analytical methodology," *IEEE Access*, vol. 8, pp. 72158–72168, 2020.

[5] T.-L. Wang, D. Huang, and M. Shahawy, "Dynamic response of multigirder bridges," *Journal of Structural Engineering*, vol. 118, no. 8, pp. 2222–2238, 1992.

[6] L. Deng and C. Cai, "Identification of dynamic vehicular axle loads: demonstration by a field study," *Journal of Vibration and Control*, vol. 17, no. 2, pp. 183–195, 2011.

[7] Y. B. Yang, M. C. Cheng, and K. C. Chang, "Frequency variation in vehicle–bridge interaction systems," *International Journal of Structural Stability and Dynamics*, vol. 13, no. 02, Article ID 1350019, 2013.

[8] M. Wu, Y. Li, and W. Zhang, "Impacts of wind shielding effects of bridge tower on railway vehicle running performance," *Wind and Structures*, vol. 25, no. 1, pp. 63–77, 2017.

[9] H. Li, Z. Yu, J. Mao, and B. F. Spencer, "Effect of seismic isolation on random seismic response of High-Speed railway bridge based on probability density evolution method," *Structures*, vol. 29, pp. 1032–1046, 2021.

[10] M.-H. Tsai, S.-Y. Wu, K.-C. Chang, and G. C. Lee, "Shaking table tests of a scaled bridge model with rolling-type seismic isolation bearings," *Engineering Structures*, vol. 29, no. 5, pp. 694–702, 2007.

[11] M. Ma, M. Li, X. Qu, and H. Zhang, "Effect of passing metro trains on uncertainty of vibration source intensity: monitoring tests," *Measurement*, Article ID 110992, 2022.

[12] L. Xu and M. Ma, "Dynamic response of the multilayered half-space medium due to the spatially periodic harmonic moving load," *Soil Dynamics and Earthquake Engineering*, Article ID 107246, 2022.

[13] C. Zou, J. A. Moore, M. Sanayei, and Y. Wang, "Impedance model for estimating train-induced building vibrations," *Engineering Structures*, vol. 172, pp. 739–750, 2018.

[14] J. Wu, F. Cheng, C. Zou et al., "Swarm intelligent optimization conjunction with kriging model for bridge structure finite element model updating," *Buildings*, vol. 12, no. 5, p. 504, 2022.

[15] M. Brennan, "Some recent developments on adaptive tuned vibration absorbers/neutralisers (Invited Keynote Study)," in *Proceedings of the XI DINAME*, Ouro Preto, MG, Brazil, July 2005.

[16] C. C. Lin, G. L. Lin, and J. F. Wang, "Protection of seismic structures using semi-active friction TMD," *Earthquake Engineering & Structural Dynamics*, vol. 39, no. 6, pp. 635–659, 2010.

[17] A. R. Magnuson, "Mitigation of traffic-induced bridge vibrations through passive and semi-active control devices," Doctoral dissertation, Massachusetts Institute of Technology, Cambridge, MA, USA, 2011.

[18] R. Rana and T. Soong, "Parametric study and simplified design of tuned mass dampers," *Engineering Structures*, vol. 20, no. 3, pp. 193–204, 1998.

[19] J. J. Connor, *Structural Motion Control*, Pearson Education, Inc, New York, NY, USA, 2003.

[20] S. M. Nigdeli and G. Bekdaş, "Optimum tuned mass damper design in frequency domain for structures," *KSCE Journal of Civil Engineering*, vol. 21, no. 3, pp. 912–922, 2017.

[21] S. M. Nigdeli and G. Bekdas, "Optimum tuned mass damper approaches for adjacent structures," *Earthquakes and Structures*, vol. 7, no. 6, pp. 1071–1091, 2014.

[22] J. Salvi, F. Pioldi, and E. Rizzi, "Optimum tuned mass dampers under seismic soil-structure interaction," *Soil Dynamics and Earthquake Engineering*, vol. 114, pp. 576–597, 2018.

[23] G. Bekdaş and S. M. Nigdeli, "Metaheuristic based optimization of tuned mass dampers under earthquake excitation by considering soil-structure interaction," *Soil Dynamics and Earthquake Engineering*, vol. 92, pp. 443–461, 2017.

[24] G. Bekdaş, S. M. Nigdeli, and X.-S. Yang, "A novel bat algorithm based optimum tuning of mass dampers for improving the seismic safety of structures," *Engineering Structures*, vol. 159, pp. 89–98, 2018.

[25] H. Zhang and L. Zhang, "Tuned mass damper system of high-rise intake towers optimized by improved harmony search algorithm," *Engineering Structures*, vol. 138, pp. 270–282, 2017.

[26] Z. Lu, K. Li, Y. Ouyang, and J. Shan, "Performance-based optimal design of tuned impact damper for seismically excited nonlinear building," *Engineering Structures*, vol. 160, pp. 314–327, 2018.

[27] S. M. Nigdeli and G. Bekdaş, "Optimum design of multiple positioned tuned mass dampers for structures constrained with axial force capacity," *The Structural Design of Tall and Special Buildings*, vol. 28, no. 5, 2019.

[28] G. Bekdaş, A. E. Kayabekir, S. M. Nigdeli, and Y. C. Toklu, "Tranfer function amplitude minimization for structures with tuned mass dampers considering soil-structure interaction," *Soil Dynamics and Earthquake Engineering*, vol. 116, pp. 552–562, 2019.

[29] W. Shen, S. Zhu, Y. L. Xu, and H. p. Zhu, "Energy regenerative tuned mass dampers in high-rise buildings," *Structural Control and Health Monitoring*, vol. 25, no. 2, 2018.

[30] W.-a. Shen, S. Zhu, and Y.-l. Xu, "An experimental study on self-powered vibration control and monitoring system using electromagnetic TMD and wireless sensors," *Sensors and Actuators A: Physical*, vol. 180, pp. 166–176, 2012.

[31] R. Jabary and S. Madabhushi, "Structure-soil-structure interaction effects on structures retrofitted with tuned mass dampers," *Soil Dynamics and Earthquake Engineering*, vol. 100, pp. 301–315, 2017.

[32] M. De Angelis, S. Perno, and A. Reggio, "Dynamic response and optimal design of structures with large mass ratio TMD," *Earthquake Engineering & Structural Dynamics*, vol. 41, no. 1, pp. 41–60, 2012.

[33] Q. Wang, X. Dong, L. Li, and J. Ou, "Study on an improved variable stiffness tuned mass damper based on conical

magnetorheological elastomer isolators," *Smart Materials and Structures*, vol. 26, no. 10, Article ID 105028, 2017.

[34] Z. Lu, X. Chen, D. Zhang, and K. Dai, "Experimental and analytical study on the performance of particle tuned mass dampers under seismic excitation," *Earthquake Engineering & Structural Dynamics*, vol. 46, no. 5, pp. 697–714, 2017.

[35] Z. Lu, B. Huang, Q. Zhang, and X. Lu, "Experimental and analytical study on vibration control effects of eddy-current tuned mass dampers under seismic excitations," *Journal of Sound and Vibration*, vol. 421, pp. 153–165, 2018.

[36] X. Yin, Y. Liu, G. Song, and Y. L. Mo, "Suppression of bridge vibration induced by moving vehicles using pounding tuned mass dampers," *Journal of Bridge Engineering*, vol. 23, no. 7, Article ID 04018047, 2018.

[37] J. Jiang, P. Zhang, D. Patil, H. N. Li, and G. Song, "Experimental studies on the effectiveness and robustness of a pounding tuned mass damper for vibration suppression of a submerged cylindrical pipe," *Structural Control and Health Monitoring*, vol. 24, no. 12, Article ID e2027, 2017.

[38] X. Yin, G. Song, and Y. Liu, "Vibration suppression of wind/traffic/bridge coupled system using multiple pounding tuned mass dampers (MPTMD)," *Sensors*, vol. 19, no. 5, p. 1133, 2019.

[39] W. Wang, X. Wang, X. Hua, G. Song, and Z. Chen, "Vibration control of vortex-induced vibrations of a bridge deck by a single-side pounding tuned mass damper," *Engineering Structures*, vol. 173, pp. 61–75, 2018.

[40] H. Li, P. Zhang, G. Song, D. Patil, and Y. Mo, "Robustness study of the pounding tuned mass damper for vibration control of subsea jumpers," *Smart Materials and Structures*, vol. 24, no. 9, Article ID 095001, 2015.

[41] P. Zhang, G. Song, H.-N. Li, and Y.-X. Lin, "Seismic control of power transmission tower using pounding TMD," *Journal of Engineering Mechanics*, vol. 139, no. 10, pp. 1395–1406, 2013.

[42] L. Tian and X. Gai, "Wind-induced vibration control of power transmission tower using pounding tuned mass damper," *Journal of Vibroengineering*, vol. 17, no. 7, pp. 3693–3701, 2015.

[43] W. Lin, Q. Wang, J. Li, S. Chen, and A. Qi, "Shaking table test of pounding tuned mass damper (PTMD) on a frame structure under earthquake excitation," *Computers and Concrete, An International Journal*, vol. 20, no. 5, pp. 545–553, 2017.

[44] G. B. Song, P. Zhang, L. Y. Li et al., "Vibration control of a pipeline structure using pounding tuned mass damper," *Journal of Engineering Mechanics*, vol. 142, no. 6, Article ID 04016031, 2016.

[45] P. Zhang, J. Tan, H. Liu, G. Yang, and C. Cui, "Seismic vibration mitigation of a cable-stayed bridge with asymmetric pounding tuned mass damper," *Mathematical Problems in Engineering*, Advance online publication, vol. 2021, 2021.

[46] S. Chen and J. Wu, "Performance enhancement of bridge infrastructure systems: long-span bridge, moving trucks and wind with tuned mass dampers," *Engineering Structures*, vol. 30, no. 11, pp. 3316–3324, 2008.